

$p\kappa$ -Curves: Interpolatory curves with curvature approximating a parabola

Zhihao Wang^{a,b}, Juan Cao^{a,b,*}, Tuan Guan^{a,b}, Zhonggui Chen^c, Yongjie Jessica Zhang^d

^a*School of Mathematical Sciences, Xiamen University, Xiamen, Fujian, 361005, China*

^b*Fujian Provincial Key Laboratory of Mathematical Modeling and High-Performance Scientific Computation, Xiamen University, Xiamen, Fujian, 361005, China*

^c*School of Informatics, Xiamen University, Xiamen, Fujian, 361005, China*

^d*Department of Mechanical Engineering, Carnegie Mellon University, Pittsburgh, PA 15213, USA*

Abstract

This paper introduces a novel class of fair and interpolatory curves called $p\kappa$ -curves. These curves are comprised of smoothly stitched Bézier curve segments, where the curvature distribution of each segment is made to closely resemble a parabola, resulting in an aesthetically pleasing shape. Moreover, each segment passes through an interpolated point at a parameter where the parabola has an extremum, encouraging the alignment of interpolated points with curvature extrema. To achieve these properties, we tailor an energy function that guides the optimization process to obtain the desired curve characteristics. Additionally, we develop an efficient algorithm and an initialization method, enabling interactive modeling of the $p\kappa$ -curves without the need for global optimization. We provide various examples and comparisons with existing state-of-the-art methods to demonstrate the curve modeling capabilities and visually pleasing appearance of $p\kappa$ -curves.

Keywords: Fairness, interpolation, continuity, smoothness, locality

1. Introduction

Interpolatory curves play a crucial role in computer-aided geometric design (CAGD) and find extensive applications in various fields such as industrial design, art design, shape representation, animation, and more (Farin, 2002). Piecewise parametric curves are commonly employed to design complex shapes due to their flexibility (Piegl and Tiller, 1996). As a result, the construction of piecewise interpolation curves has become a popular research topic. In addition to the fundamental requirement of interpolation, there is often a need to satisfy additional geometric properties such as smoothness, locality, fairness, robustness, roundness, extensionality, and more (Levien, 2009). Among these properties, smoothness, fairness, and locality are considered key geometric properties that are highly desired in practical curve design (Binninger and Sorkine-Hornung, 2022; Wang and Zhang, 2010).

In curve design, achieving smooth and visually appealing transitions between curve segments is important. The smoothness is typically evaluated through two types of continuity: parametric continuity (C^n -continuity) and geometric continuity (G^n -continuity). C^n -continuity requires the matching of parametric derivatives up to order n at joints where the curve segments are stitched together. On the other hand, G^n -continuity demands the existence of some reparameterization of the segments, resulting in C^n -continuity at the joints. The choice of continuity order depends on the specific application. In many cases, achieving second-order continuity (C^2 - or G^2 -continuity) is desirable in curve design with multiple segments due to its practical and aesthetic benefits (Sederberg, 2012).

The concept of fairness in curve design is subjective and lacks a precise mathematical criterion for evaluation. However, studies in psychology have shown that the fairness of a curve is strongly correlated

*Corresponding author

Email address: juancao@xmu.edu.cn (Juan Cao)

with its curvature (Attneave, 1954; Levien, 2009). Curves that exhibit smooth curvature variation and have fewer curvature monotonic intervals are commonly associated with a perception of having a more fairing shape (Farin, 2002). Previous methods have commonly emphasized the necessity of maintaining monotonic curvature variation on each curve segment to enhance the smoothness and aesthetic quality of curves (Mineur et al., 1998; Cao and Wang, 2008). However, in curve construction with multiple segments, achieving both smoothness and fairness in higher-order curves poses challenges due to the intricate task of preserving curvature monotonicity while handling non-unique curvature extreme points. In addressing the fairing problem, some other approaches formulate it as an energy optimization problem (Zhang et al., 2001; Levien and Séquin, 2009; Jiang et al., 2023). However, these approaches do not explicitly consider curvature features such as monotonicity and the position of local curvature extremes.

The locality property of curves means that changes in the position of an interpolated point only affect its adjacent region of the curve. This enables easier and more intuitive local adjustments to the curve shape, allowing users to fine-tune specific regions of interest. Additionally, it improves computational efficiency by limiting calculations to the affected local portions of the curve, reducing complexity and speeding up the curve editing process. In general, there is a tradeoff between achieving locality and higher-order continuity, i.e. curves with higher-order continuity usually have weaker locality (Levien and Séquin, 2009). In particular, methods that construct curves relying on global optimization techniques typically do not exhibit locality.

To design interpolatory curves with complex shapes, geometric primitives such as (rational) Bézier curves (Yan et al., 2017, 2019), trigonometric blending curves (Yuksel, 2020), clothoids and straight lines (Binninger and Sorkine-Hornung, 2022) are commonly used. In this paper, we propose an efficient method for constructing 2D interpolatory curves that satisfy three specific properties (smoothness, fairness, and locality), using quartic and quintic Bézier curves as the geometric primitives. Different from the traditional criterion of monotonic curvature variation, our approach focuses on encouraging each segment to closely approximate a parabolic shape in terms of curvature variation. Additionally, we align the interpolation point with the extreme value of the approximated parabola. Compared to the previous energy optimization approaches, the resulting curve segments tend to have a maximum of two monotonic intervals in terms of curvature variation. This approach leads to fairing interpolatory curve designs. We introduce “ $p\kappa$ -curves” to refer to these constructed curves, which consist of segments with approximate parabolic curvature variations. Our specific contributions are as follows:

- We propose an optimization-based method for constructing fair and interpolatory $p\kappa$ -curves using Bézier segments. We have tailored an energy function to guide the optimization process and obtain these curves. The resulting $p\kappa$ -curves exhibit several desirable properties, such as a curvature distribution in each segment that closely resembles a parabola, interpolated points closely aligning with curvature extrema, up to C^2/G^2 smoothness, and a strong locality property.
- We develop an efficient algorithm for locally solving the optimization problem. This algorithm is equipped with an efficient initialization method, enabling interactive design and local editing. Experimental results demonstrate the capability of our method in diverse shape design, producing aesthetically pleasing curves.

The paper is organized as follows: Section 2 provides a review of the related works on interpolatory curves. Section 3 offers a brief introduction to the definition, calculation, properties, and notation of Bézier curves. The optimization problem for the construction of $p\kappa$ -curves is presented in Section 4. The optimization method for interactive interpolatory curve design is given in Section 5. Section 6 conducts an ablation study, presents the experimental results, and provides a comparison with state-of-the-art methods. Finally, Section 7 concludes the paper.

2. Related work

Extensive research has focused on constructing interpolatory curves using multiple geometric primitives. According to the primitives used, these methods can be categorized into three groups: polynomial curves

(including their rational forms), logarithmic aesthetic curves, and blending of different primitives. For a comprehensive survey on this topic, please refer to (Hoschek et al., 1993; Levien, 2009; Miura and Gobithaasan, 2014).

2.1. Polynomial curves

Polynomial representations like Bézier, B-spline, and NURBS have found widespread use in constructing free-form curves within Computer-Aided Geometric Design (CAGD) (Piegl and Tiller, 1996). These representations have gained popularity due to their simplicity and intuitive controls. Researchers have proposed different types of smooth interpolation curves, such as Catmull-Rom splines (Catmull and Rom, 1974; Barry and Goldman, 1988), G^2 cubic splines (Farin, 2002) and subdivision curves (Deslauriers and Dubuc, 1989). However, the main focus of these earlier works has been on achieving smoothness and accurate interpolation, with less consideration given to curve fairness, resulting in unexpected geometric feature points (cusps, inflections, and loops).

κ -curves, introduced by Yan et al. (2017), offer improved control over the curvature distribution of interpolatory curves. These curves are constructed by connecting a series of quadratic Bézier curve segments, where each segment is specifically designed to have its unique curvature maximum aligned with a given point. This concept was later extended through the utilization of rational quadratic Bézier curves, enabling accurate representation of circles, as well as other elliptical or hyperbolic shapes (Yan et al., 2019). $\epsilon\kappa$ -curves (Miura et al., 2022) are another extension of the κ -curves that employ cubic Bézier curves. By utilizing higher-degree primitives, $\epsilon\kappa$ -curves introduce additional degrees of freedom (DOFs), enabling precise control over the magnitudes of local maximum curvature. Due to their reliance on global optimization techniques, κ -curves and their generalizations lack locality. Additionally, because the number of DOFs is limited, neither κ -curves nor their generalizations can guarantee global second-order continuity. The feature points controlled interpolatory curves (FPC-curves) also utilize cubic Bézier curves, with a primary objective of efficiently and precisely controlling the location and type of geometric feature points (Chen et al., 2019). FPC-curves exhibit good local properties, but at joints where there is a sign change in curvature, the continuity is reduced to G^1 . Directly utilizing higher-order polynomial primitives provides increased DOFs for achieving higher-order continuity. However, it also increases the difficulty in controlling curvature variation due to the presence of multiple curvature extrema within each high-order segment.

Alternatively, several research works have focused on obtaining fair curves by minimizing specific energy functions tailored for polynomial representation. These energy functions include stretch energy (Xu et al., 2011), strain energy (Chan et al., 2011; Xu et al., 2011), jerk energy (ERİŞKİN and YÜCESAN, 2016; Xu et al., 2011), bending energy (Johnson and Johnson, 2020), and others. These energy functions are generally defined globally, which would lead to curves that lack locality. In a recent work, Jiang et al. (2023) employed the progressive iterative approximation method for fairing curve construction, allowing for local improvements. However, none of these methods directly considers the variation of curvature or the positions of local curvature extrema.

2.2. Log-aesthetic curves

Log-aesthetic curves (LACs) are visually pleasing curves with linear curvature and torsion graphs, resulting in a monotonically varying curvature (Miura et al., 2005). These curves are highly valued in aesthetic design, and previous research has developed smooth interpolation curves based on log-aesthetic curves (Miura et al., 2013; Wang et al., 2020). LACs include well-known curves such as the logarithmic spiral, clothoid, and involute of a circle. Among them, the clothoid (Euler spiral) has a linear variation of curvature with respect to arc length, making it suitable for achieving local maximum curvature at interpolated points. Extensive research has been conducted on constructing clothoid-based interpolated curves using global optimization methods, such as (Havemann et al., 2013; Bertolazzi and Frego, 2018). More recently, Binninger and Sorkine-Hornung (2022) proposed a planar curve comprised of piecewise clothoids and straight lines, allowing local shape control by adjusting the position of interpolated points and re-estimating the associated curvatures. It is worth noting that LACs generally lack a closed-form representation as they are defined via Fresnel integrals (Olver, 2010). Hence, numerical methods are commonly employed for curve construction and computation of values and derivatives.

2.3. Blending curves

Blending curves are constructed by combining different types of geometric primitives, such as (rational) Bézier curves, (rational) B-spline curves, line segments, parabolas, and circle arcs. In early works on blending curve construction, the main emphasis was on achieving G^1 -continuity in interpolation, for example, by blending circular arcs and straight lines (Wenz, 1996) and linearly blending weight functions (Overhauser, 1968; Wenz, 1996; Pobegailo, 1992). Subsequently, considerable research efforts have focused on achieving C^2 -continuity. Wilsche (2005) introduced polynomial functions for blending two arbitrarily parametric curves. Other approaches utilize B-spline basis functions to blend Lagrange (Wilsche, 2005) or Hermite interpolants (Gferrer and Röschel, 2001). Polynomial blending functions, as presented in (Pobegailo, 2013), offer the ability to construct curves with arbitrarily high orders of continuity. Trigonometric blending functions have also been applied in interpolating circular arcs, as demonstrated in (Szilvási-Nagy and Vendel, 2000; Séquin et al., 2005). In (Sun and Zhao, 2009), a similar formulation using rational quadratic Bézier interpolation was introduced, allowing for the creation of conic sections. Recently, (Yuksel, 2020) introduced a method that utilizes trigonometric blending of hybrid circular-elliptical interpolations. This method constructs curves that are free from cusps or self-intersections between two consecutive interpolated points. While all these blending curves exhibit locality and computational efficiency, they do not take into account the variation of curvature and the position of curvature extrema.

3. Preliminary

In this section, we provide a brief introduction to the definitions, calculations, properties, and notations of Bézier curves, which are relevant to our study.

3.1. Bézier curves

In this paper, we utilize Bézier curves as the geometric primitives for constructing our interpolatory curves. Assume an interpolatory curve $\{\mathcal{P}_{i,k}(t)\}_{i=0}^m$ consists of $m + 1$ degree- k Bézier segments. The i -th segment of the parametric curve sequence can be defined as follows:

$$\mathcal{P}_{i,k}(t) = \sum_{j=0}^k \mathbf{c}_{i,j} B_j^k(t), \quad t \in [0, 1], \quad (1)$$

where $\mathbf{c}_{i,j} \in \mathbb{R}^2$ are the control points and $B_j^k(t)$ denotes the degree- k Bernstein base function given by

$$B_j^k(t) = \frac{k!}{j!(k-j)!} t^j (1-t)^{k-j}.$$

The polyline formed by sequentially connecting the control points $\mathbf{c}_{i,j}$ ($j = 0, \dots, k$) is referred to as the control polygon of the Bézier curve $\mathcal{P}_{i,k}(t)$. The curvature of $\mathcal{P}_{i,k}(t)$ can be computed as follows:

$$\kappa_i(t) = \frac{\det(\mathcal{P}'_{i,k}(t), \mathcal{P}''_{i,k}(t))}{\|\mathcal{P}'_{i,k}(t)\|^3}, \quad (2)$$

where $\det(\cdot)$ represents the determinant of a matrix, \cdot' and \cdot'' denotes the first and second derivative operations, and $\|\cdot\|$ denotes the length of a vector.

3.2. Degree elevation and subdivision

Bézier curves have found extensive applications in CAGD, owing to the development of various effective algorithms (Farin, 2002). In this paper, we adopt the degree elevation algorithm and subdivision algorithm, which we briefly review here.

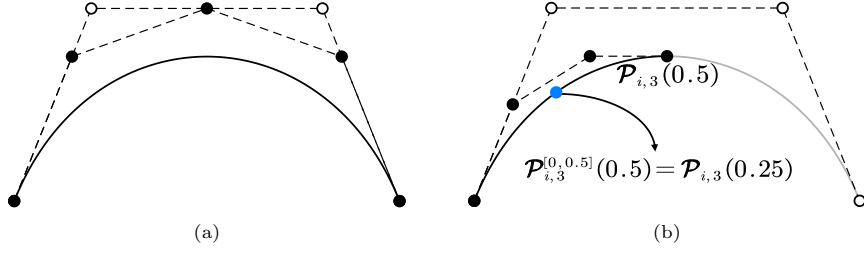


Figure 1: Bézier curve degree elevation and subdivision. (a) Degree elevation of a cubic Bézier curve to quartic, and (b) subdivision of Bézier curve $\mathcal{P}_{i,3}(t)$ at $t = z = 0.5$ and the left segment $\mathcal{P}_{i,3}^{[0,0.5]}(\bar{t}) = \mathcal{P}_{i,3}(\bar{t}/2)$, $\bar{t} \in [0, 1]$. Original control points are denoted by hollow points, while control points after the degree elevation and subdivision operations are indicated by solid points.

Degree elevation. The degree elevation algorithm is used to calculate the control points $\bar{c}_{i,j}$ of a degree- $(k+1)$ Bézier curve

$$\mathcal{P}_{i,k+1}(t) = \sum_{j=0}^{k+1} \bar{c}_{i,j} B_j^k(t), \quad t \in [0, 1],$$

that is geometrically and parametrically equivalent to a given degree- k Bézier curve $\mathcal{P}_{i,k}(t)$ defined in Eq. (1), where the control points are:

$$\bar{c}_{i,0} = c_{i,0}; \quad \bar{c}_{i,l} = \frac{l}{k+1} c_{i,l-1} + \left(1 - \frac{l}{k+1}\right) c_{i,l}, \quad l = 1, \dots, k; \quad \bar{c}_{i,k+1} = c_{i,k}.$$

In Fig. 1(a), we present an example of a curve, showing the control points both before and after the degree elevation process.

Subdivision. The subdivision algorithm can be used to split a given curve defined in Eq. (1) at parameter $t = z$ ($z \in (0, 1)$) into two curve segments $\mathcal{P}_{i,k}^{[0,z]}(\bar{t})$ and $\mathcal{P}_{i,k}^{[z,1]}(\bar{t})$, each of which is still a Bézier curve. In particular, the segment of the curve on $[0, z]$ is geometrically equivalent to a degree- k Bézier curve

$$\mathcal{P}_{i,k}^{[0,z]}(\bar{t}) = \sum_{j=0}^k \bar{c}_{i,j} B_j^k(\bar{t}), \quad \bar{t} \in [0, 1],$$

where the control points can be computed as

$$\begin{bmatrix} \bar{c}_{i,0} \\ \bar{c}_{i,1} \\ \dots \\ \bar{c}_{i,k} \end{bmatrix} = \begin{pmatrix} 1, & 0, & \dots & 0 \\ 1-z, & z, & \dots & 0 \\ \dots & \vdots & \dots & \vdots \\ (1-z)^k, & \frac{k(k-1)}{2}(1-z)^{(k-1)}z, & \dots & z^k \end{pmatrix} \begin{bmatrix} c_{i,0} \\ c_{i,1} \\ \dots \\ c_{i,k} \end{bmatrix}.$$

A point on the original curve with a parameter value $t \in [0, z]$ corresponds to a new parameter value $\bar{t} = t/z$ on the new representation, specifically $\mathcal{P}_{i,k}^{[0,z]}(\bar{t}) = \mathcal{P}_{i,k}(t)$. In Fig. 1(b), we demonstrate Bézier subdivision, splitting the original curve at $t = 0.5$, where we have $\mathcal{P}_{i,k}^{[0,z]}(\bar{t}) = \mathcal{P}_{i,k}(\bar{t}/2)$. By applying the symmetry property of the Bézier curve, we can also determine the control points for the segment $\mathcal{P}_{i,k}^{[z,1]}(\bar{t})$ on $[z, 1]$.

3.3. Continuity constrains

When constructing interpolatory curves using Bézier curves, achieving higher-order continuity at the joining points is crucial as it greatly impacts the aesthetic quality of the curve shape. There are two types of continuity in Bézier curves: parametric continuity (C^n) and geometric continuity (G^n). Parametric continuity emphasizes smoothness in the curve's parameterization, while geometric continuity focuses on visual

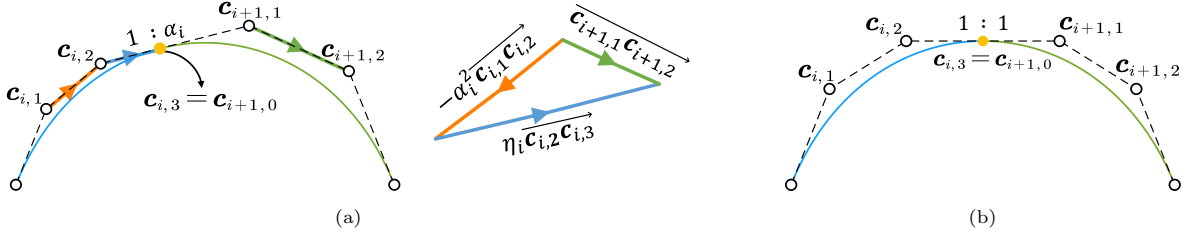


Figure 2: G^2 - and C^2 -continuity constraints for Bézier Curves. The two curves are colored in blue and green, respectively. (a) G^2 -continuity, where the control legs of the two curves at the joint (yellow point) are collinear with a length ratio of $1 : \alpha_i$. Additionally, the last two control legs of the left curve, scaled by factors $-\alpha_i^2$ and η_i respectively, form a triangle with the second control leg of the right curve. (b) C^2 -continuity, a specific case of (a) with $\alpha_i = 1$ and $\eta_i = 2$.

smoothness in the curve's shape. Given the adjacent Bézier curves $\mathcal{P}_{i,k}(t)$, $\mathcal{P}_{i+1,k}(t)$, the constraints for ensuring C^n and G^n -continuity at the joint $\mathcal{P}_{i,k}(1) = \mathcal{P}_{i+1,k}(0)$ are denoted as $C_i^{C,n}$ and $C_i^{G,n}$, respectively. Specifically, the constraints for achieving first-order and second-order continuities in the 2D plane are as follows (Sederberg, 2012):

- $C_i^{C,1}$: $\mathbf{c}_{i,k} = \mathbf{c}_{i+1,0}$ and $\mathbf{c}_{i,k} - \mathbf{c}_{i,k-1} = \mathbf{c}_{i+1,1} - \mathbf{c}_{i+1,0}$.
- $C_i^{C,2}$: $C_i^{C,1}$ and $\mathbf{c}_{i,k-2} - 2\mathbf{c}_{i,k-1} = \mathbf{c}_{i+1,2} - 2\mathbf{c}_{i+1,1}$.
- $C_i^{G,1}$: $\mathbf{c}_{i,k} = \mathbf{c}_{i+1,0}$ and $\exists \alpha_i > 0$ s.t. $\alpha_i(\mathbf{c}_{i,k} - \mathbf{c}_{i,k-1}) = \mathbf{c}_{i+1,1} - \mathbf{c}_{i+1,0}$.
- $C_i^{G,2}$: $C_i^{G,1}$ and $\exists \eta_i \in \mathbb{R}$ s.t. $-\alpha_i^2(\mathbf{c}_{i,k-1} - \mathbf{c}_{i,k-2}) + \eta_i(\mathbf{c}_{i,k} - \mathbf{c}_{i,k-1}) = \mathbf{c}_{i+1,2} - \mathbf{c}_{i+1,1}$.

The constraints for achieving G^2 - and C^2 -continuity between two Bézier curves at their joint are shown in Fig. 2. For a more in-depth discussion on parametric and geometric continuity, we recommend referring to (Farin, 2002).

4. Problem statement

In this section, we define the optimization problem for constructing $p\kappa$ -curves, including the key objectives and constraints.

4.1. Constraints

We start by discussing the constraints for constructing an open interpolatory curve. Given an ordered set of points $\{\mathbf{p}_i\}_{i=0}^{n+1}$ ($n \geq 1$), our objective is to create a curve composed of n parametric curves $\{\mathcal{P}_{i,k}(t)\}_{i=1}^n$. The first curve segment should begin at the first interpolated point \mathbf{p}_0 , and the last curve segment should end at the last interpolated point \mathbf{p}_{n+1} . We denote this end condition by C^E , i.e.,

- C^E : $\mathbf{c}_{1,0} = \mathbf{p}_0$, $\mathbf{c}_{n,k} = \mathbf{p}_{n+1}$.

Then, each curve segment $\mathcal{P}_{i,k}$ ($1 \leq i \leq n$) is required to interpolate the corresponding point \mathbf{p}_i at a suitable parameter value t_i ; see Fig. 3(a). We denote this position interpolation constraints as C_i^I , which can be defined as follows:

- C_i^I : $\mathcal{P}_{i,k}(t_i) = \sum_{j=0}^k \mathbf{c}_{i,j} B_j^k(t_i) = \mathbf{p}_i$, $t_i \in [0, 1]$, $i = 1, \dots, n$.

The selection of t_i in the above constraints and its initialization will be discussed in Section 4.2 and Section 5.2, respectively. Additionally, each adjacent curve pair must be smoothly connected by satisfying either parametric or geometric continuity constraints listed in Section 3.3. When constructing a closed interpolatory curve, two additional adjacent segments, denoted as $\mathcal{P}_{0,k}$ and $\mathcal{P}_{n+1,k}$ and positioned between $\mathcal{P}_{1,k}$ and

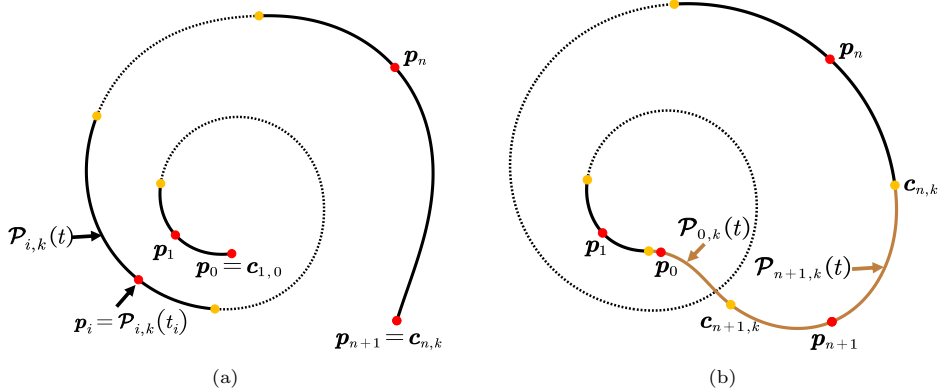


Figure 3: Constraints for constructing interpolatory curves. (a) Open curve satisfying end condition C^E and interpolation condition C_i^I , $i = 1, \dots, n$, and (b) closed curve with two additional adjacent segments, $\mathcal{P}_{0,k}$ and $\mathcal{P}_{n+1,k}$ (marked in brown), satisfying interpolation condition C_i^I , $i = 0, \dots, n+1$. The red and yellow points represent the interpolated points and joints of Bézier segments, respectively.

$\mathcal{P}_{n,k}$, are included; see Fig. 3(b). The end condition C^E is then replaced with two position interpolation constraints, namely C_0^I and C_{n+1}^I .

Note that achieving higher-order continuity requires more control points compared to lower-order continuity. In our application, we utilize quartic (resp. quintic) Bézier curves $\mathcal{P}_{i,4}$ (resp. $\mathcal{P}_{i,5}$) for constructing G^1 or C^1 (resp. G^2 or C^2) interpolatory curves. This choice allows for the inclusion of more control points, which are necessary to satisfy the constraints for achieving the desired continuity, while also providing additional degrees of freedom to improve the fairness of the curve. Next, we introduce the energy function and employ optimization techniques to adjust the control points of $\mathcal{P}_{i,k}$.

4.2. Objective function

In the context of parametric curves, achieving a fair appearance is commonly associated with having a small monotonic interval of curvature and smooth curvature variation (Mineur et al., 1998; Farin, 2002). Previous methods have focused on designing curves with monotonic curvature variations to achieve fairness (Mineur et al., 1998; Cao and Wang, 2008). However, in the case of shape design using composed curves, it may not be necessary for each segment to have monotonic curvature. When considering the entire curve from a global perspective, it is unavoidable for complex geometric shapes to introduce many local curvature maxima. On the other hand, many aesthetically pleasing curves exhibit curvature plots that closely resemble a parabola (Tsuchie, 2023). Inspired by this observation, we propose a criterion for constructing a fairing composed Bézier curve, where each segment curve $\mathcal{P}_{i,k}$ closely approximates a specific parabola $\mathcal{Q}_i(t)$ in terms of curvature. The criterion encourages the curve to have at most two monotonic intervals and an extreme value in the curvature plot.

Note that, the curvature function of a Bézier curve is non-polynomial in terms of the parameter t . Hence, it is not possible to construct a Bézier curve whose curvature perfectly follows a parabolic function due to the inherent differences in their mathematical representations. To overcome this limitation, we employ optimization techniques to adjust the control points of $\mathcal{P}_{i,k}$ in order to approximate the desired parabolic curvature distribution. In order to achieve this objective, we formulate energy functions that consist of three different types of terms:

- **Parabolic curvature term.** The first type of terms captures the discrepancy between the actual curvature of $\mathcal{P}_{i,k}$ and a parabola $\mathcal{Q}_i(t)$, which can be expressed as follows:

$$E_{i,p}(c_{i,0}, \dots, c_{i,k}, a_{i,0}, a_{i,1}, a_{i,2}) = \int_0^1 (\kappa_i(t) - \mathcal{Q}_i(t))^2 \|\mathcal{P}'_{i,k}(t)\| dt, \quad (3)$$

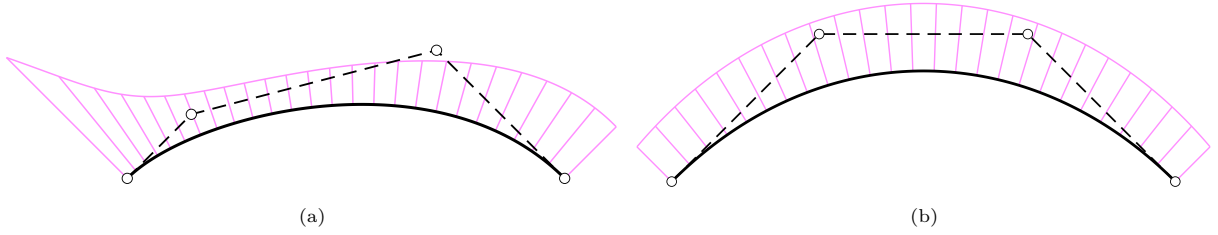


Figure 4: The influence of the control polygon shape on the curvature distribution of cubic Bézier curves. The curves in (a) and (b) have control polygons (dashed lines) with varying and similar edge lengths, respectively. The quality of the curves is visualized using the curvature comb colored in pink.

where $\mathcal{Q}_i(t) = a_{i,0} + a_{i,1}t + a_{i,2}t^2$ represents the parabola to be approximated by the curvature $\kappa_i(t)$, and $\|\mathcal{P}'_{i,k}(t)\|dt$ is the differential of arc length of the curve segment $\mathcal{P}_{i,k}$.

- **Edge length regularization term.** In fairing curve design, it is important to consider the lengths of adjacent edges of the Bézier control polygon. For instance, in typical curves (Mineur et al., 1998; Tong and Chen, 2021) or Class A curves (Farin, 2006; Cao and Wang, 2008), which are characterized by monotonic curvature variation, the lengths of adjacent control legs are uniformly scaled. However, when a relatively large scaling factor is employed, the curves, despite displaying a monotonic variation in curvature, might appear almost straight in certain sections. In Fig. 4(a), we can observe that when the edge length of the control polygon in a Bézier curve varies, the curvature tends to exhibit more changes. Conversely, when the edges of the control polygon have similar lengths, the curvature varies more smoothly; see Fig. 4(b). Hence, the second type of terms in our energy functions restricts the variation in length between adjacent edges of a Bézier curve. This restriction is defined as follows:

$$E_{i,e}(\mathbf{c}_{i,0}, \dots, \mathbf{c}_{i,k}) = \sum_{j=0}^{k-2} (\|\mathbf{c}_{i,j} - \mathbf{c}_{i,j+1}\|^2 - \|\mathbf{c}_{i,j+1} - \mathbf{c}_{i,j+2}\|^2)^2. \quad (4)$$

- **Curve length term.** In our application, it is desirable to avoid curve segments with large arc lengths. Instead of directly penalizing the arc length of the curve, we address this issue by incorporating an energy term that penalizes the length of the control polygon. The definition of this energy term is as follows:

$$E_{i,c}(\mathbf{c}_{i,0}, \dots, \mathbf{c}_{i,k}) = \sum_{j=0}^{k-1} \|\mathbf{c}_{i,j} - \mathbf{c}_{i,j+1}\|^2. \quad (5)$$

In summary, the optimization problem for constructing open C^2 -continuous quintic $p\kappa$ -curves $\{\mathcal{P}_{i,5}(t)\}_{i=1}^n$ can be formulated as follows:

$$\begin{aligned} \min_{\mathbf{c}_{i,j}, a_{i,l}} \sum_{i=1}^n E_i &= \min_{\mathbf{c}_{i,j}, a_{i,l}} \sum_{i=1}^n (E_{i,p} + \lambda_{i,e} E_{i,e} + \lambda_{i,c} E_{i,c}) \\ \text{s.t. constraints } C^E, \{C_i^I\}_{i=1}^n, \text{ and } \{C_i^{C,2}\}_{i=1}^n &\text{ are satisfied,} \end{aligned} \quad (6)$$

where $j = 0, 1, \dots, 5$, $l = 0, 1, 2$, and the weights $\lambda_{i,e}$ and $\lambda_{i,c}$ are used to balance between the energy terms. The optimization problem for constructing open or closed C^1, G^1, G^2 -continuous $p\kappa$ -curves can be formulated by adapting the curve order and constraints in Eq. (6) to match the desired continuity and open/closed conditions. In the optimization process, the control points for each Bézier segment and the coefficients of the approximated parabola are treated as unknowns to be optimized. The parameter values of each interpolated point \mathbf{p}_i , are set to $t_i = -\frac{a_{i,1}}{2a_{i,2}}$, corresponding to the parameter value at which the approximated parabola achieves extrema. In our experiments, we also enforce the constraint $t_i \in [\hat{t}_i/2, (\hat{t}_i + 1)/2]$, where \hat{t}_i represents the initial value assigned to the interpolation point \mathbf{p}_i (see Section 5.2). This choice encourages the

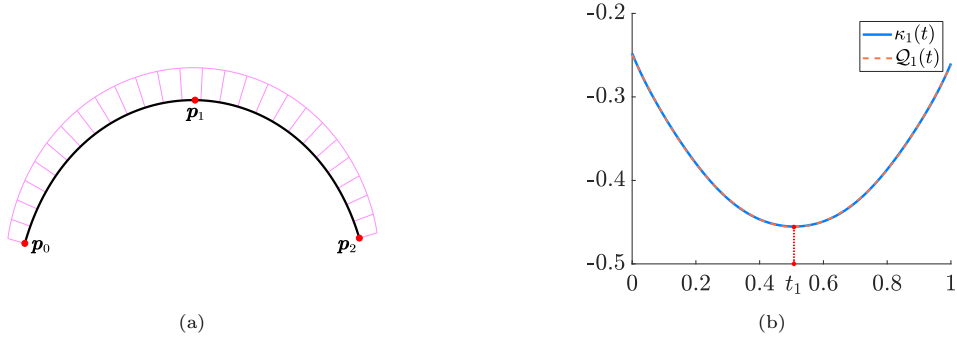


Figure 5: A toy example of an open $p\kappa$ -curve constructed from a single segment of quintic Bézier curve. (a) $p\kappa$ -curve with the curvature comb (pink) interpolating three points $\mathbf{p}_0, \mathbf{p}_1$ and \mathbf{p}_2 ; (b) curvature plot and approximated parabola. The extreme value t_1 of the parabola is selected as the parameter for the interpolation point \mathbf{p}_1 .

interpolation point \mathbf{p}_i to be located at the curvature extrema, thereby facilitating the intuitive construction of the interpolation curve by the user, as demonstrated by Yan et al. (Yan et al., 2017). Fig. 5 presents a toy example of a $p\kappa$ -curve constructed using a single segment of quintic Bézier curve, along with its corresponding curvature distribution. As depicted in Fig. 5(b), when the curvature distribution, along the curve closely resembles a parabola, it demonstrates a generally decreasing trend to the left of t_i and an increasing trend to the right of t_i . The ablation study of energy terms and the discussion about the selection of weights will be deferred until Section 6.1.

5. Local optimization method for interactive interpolatory curve design

In this section, we tackle the optimization challenge posed by the highly non-convex and non-linear problem defined in Eq. (6), which may involve a large number of unknowns. To overcome this issue, we propose a local optimization method that adjusts a small number of degrees of freedom at a time, allowing for efficient curve construction and editing (see Section 5.1). Furthermore, we present an initialization strategy and a two-stage optimization approach aimed at achieving improved suboptimal local extrema in Section 5.2 and Section 5.3, respectively.

5.1. Local construction method

In interactive design scenarios, the user may input or adjust one interpolation point at a time. Attempting to find the global optimal solution of the energy in Eq. (6) in such cases would require a global optimization from scratch, which can be computationally inefficient and may change the shape of the entire curve. To address this issue, we propose a local $p\kappa$ -curve construction algorithm. When inserting a new interpolation point, it involves adding a new Bézier segment to the existing curve. This addition only affects specific segments of the already constructed curve.

Open curve construction. Let us discuss the construction process of the open curve as an example. When $\mathbf{p}_0, \dots, \mathbf{p}_i$ ($2 \leq i \leq 3$) are inserted, we solve Eq. (6) to obtain the corresponding curve segments. Considering that $3 < i \leq n$ and $(i-1)$ -th Bézier curves have already been constructed, where $\mathbf{c}_{i-1,k} = \mathbf{p}_i$. When the $(i+1)$ -th interpolation point \mathbf{p}_{i+1} is inserted, we aim to add a Bézier curve $\mathcal{P}_{i,k}$ that satisfies the desired geometric constraints. In particular, we update only the last three Bézier curve segments $\mathcal{P}_{i-2,k}, \mathcal{P}_{i-1,k}, \mathcal{P}_{i,k}$ that interpolate points $\mathbf{p}_{i-2}, \mathbf{p}_{i-1}, \mathbf{p}_i, \mathbf{p}_{i+1}$ while keeping the segments $\mathcal{P}_{1,k}, \dots, \mathcal{P}_{i-3,k}$ fixed. The updated segments begin at the first control point $\mathbf{c}_{i-2,0}$ of segment $\mathcal{P}_{i-2,k}$ (equally, the last control point $\mathbf{c}_{i-3,k}$ of segment $\mathcal{P}_{i-3,k}$) and end at the last control point $\mathbf{c}_{i,k}$ of segment $\mathcal{P}_{i,k}$. Accordingly, we solve the following simplified optimization problem:

$$\begin{aligned}
 & \min_{\mathbf{c}_{\eta,j}, a_{\eta,l}} \sum_{\eta \in \{i-2, i-1, i\}} (E_{\eta,p} + \lambda_{\eta,e} E_{\eta,e} + \lambda_{\eta,c} E_{\eta,c}) \\
 \text{s.t. } & \mathbf{c}_{i,k} = \mathbf{p}_{i+1}, C_{i-2}^C, C_{i-1}^C, C_{i-2}^I, C_{i-1}^I \text{ and } C_i^I \text{ are satisfied,}
 \end{aligned} \tag{7}$$

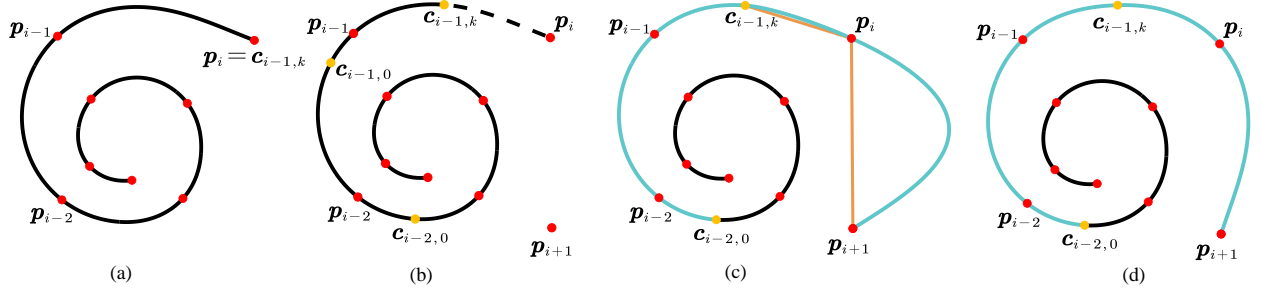


Figure 6: Local construction method for an open $p\kappa$ -curve. (a) An open $p\kappa$ -curve interpolating points $\{p_0, p_1, \dots, p_i\}$; (b) a new point p_{i+1} is inserted; (c) initialization of the open $p\kappa$ -curve interpolating $\{p_0, p_1, \dots, p_i, p_{i+1}\}$; (d) the optimized open $p\kappa$ -curve. The red and yellow points represent the interpolated points and joints of Bézier segments, respectively. Orange polylines are used for parameter value initialization. The curve segments marked in cyan are updated when the last interpolated points are inserted.

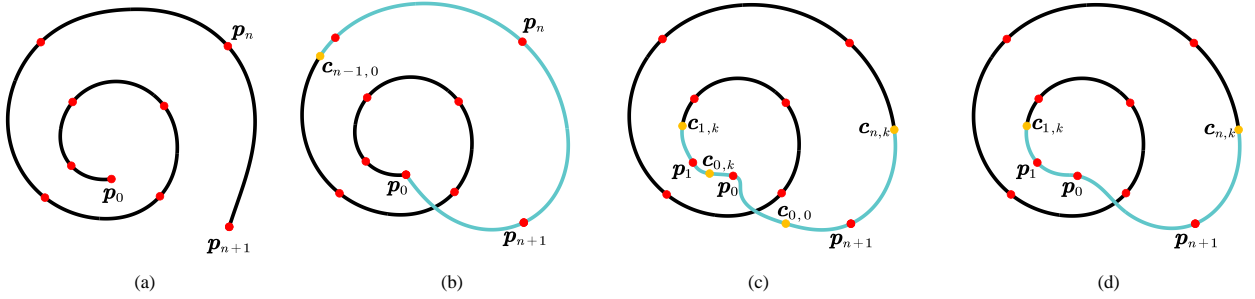


Figure 7: Local construction method for a closed $p\kappa$ -curve. (a) An open $p\kappa$ -curve interpolating points $\{p_0, p_1, \dots, p_{n+1}\}$; (b) a closed curve is constructed following the open curve construction method and treating p_0 as a point inserted after p_{n+1} ; (c) initialization of the closed $p\kappa$ -curve for segments $\mathcal{P}_{0,k}, \mathcal{P}_{1,k}, \mathcal{P}_{n+1,k}$ that interpolate p_0, p_1 and p_{n+1} , respectively; (d) the optimized closed $p\kappa$ -curve. The red and yellow points represent the interpolated points and joints of Bézier segments, respectively. The curve segments marked in cyan are updated when the open curve is closed.

where the control points of the segment $\mathcal{P}_{i-2,k}$ involved in the continuity constraints C_{i-3}^C are fixed during the optimization. Fig. 6(a) illustrates a toy example of an open C^2 -continuous quintic Bézier interpolatory curve. When the $(i+1)$ -th interpolated point is inserted, an extra Bézier segment between $c_{i-1,k}$ and p_{i+1} is introduced, which interpolates p_i ; see Fig. 6(c). The result after optimization is shown in Fig. 6(d), where the three updated segments are colored in cyan. The above process is iterated until the n -th Bézier curve $\mathcal{P}_{n,k}$ is constructed.

Closed curve construction. When constructing a closed curve interpolating points $\{p_0, \dots, p_{n+1}\}$ ($n \geq 1$), the process begins by creating an open curve following the aforementioned method. This open curve is subsequently closed to achieve the desired closed curve. Let us assume we have obtained an open curve composed of n parametric curves $\{\mathcal{P}_{i,k}(t)\}_{i=1}^n$ that interpolate points $\{p_0, \dots, p_{n+1}\}$, with the first segment $\mathcal{P}_{1,k}(t)$ starting at p_0 and the last curve segment $\mathcal{P}_{n,k}(t)$ ending at p_{n+1} ; see Fig. 7(a). By straightforwardly considering p_0 as a point inserted after p_{n+1} and solving the optimization problem described in Eq. (7), a closed curve is obtained that maintains only C^0 -continuity at the point p_0 ; see Fig. 7(b). To introduce additional degrees of freedom and achieve the desired continuity between segments, we introduce an extra segment $\mathcal{P}_{0,k}(t)$ to connect the segments $\mathcal{P}_{1,k}(t)$ and $\mathcal{P}_{n+1,k}(t)$. Then, we solve the optimization problem as

$$\begin{aligned} \min_{c_{\eta,j}, a_{\eta,l}} \sum_{\eta \in \{n+1, 0, 1\}} (E_{\eta,p} + \lambda_{\eta,e} E_{\eta,e} + \lambda_{\eta,c} E_{\eta,c}) \\ \text{s.t. } C_{n+1}^C, C_0^C, C_{n+1}^I, C_0^I \text{ and } C_1^I \text{ are satisfied,} \end{aligned} \quad (8)$$

where the control points of the segments $\mathcal{P}_{n+1,k}$ and $\mathcal{P}_{1,k}$ involved in the continuity constraints C_n^C and

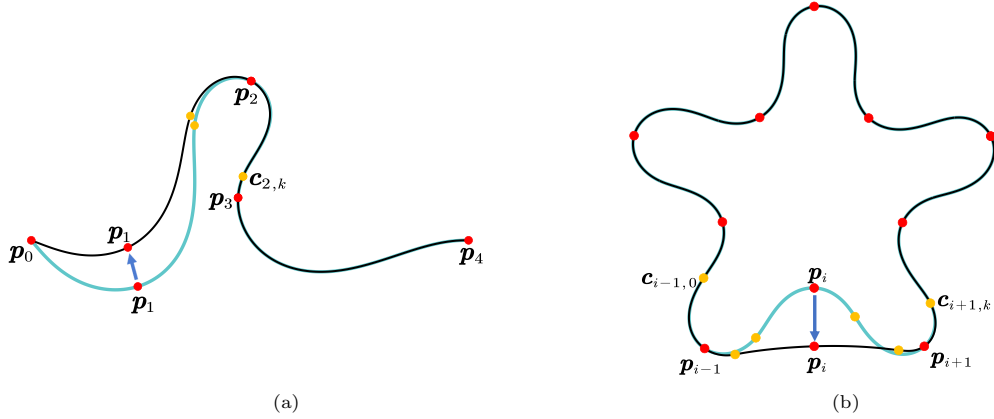


Figure 8: Local Shape Editing. (a) When moving one of the first or last two interpolation points in an open $p\kappa$ -curve, only two segments are affected. Otherwise, (b) relocating an interpolation point results in changes to three segments within the curve. Red and yellow points represent interpolated points and Bézier segment joints, respectively, while updated segments are colored in cyan.

C_1^C are fixed during the optimization. A toy example illustrating this process is shown in Fig. 7.

Local shape editing. After the construction of the entire $p\kappa$ -curve, users can make local adjustments to the shape by manipulating the position of individual interpolation points. When an interpolation point \mathbf{p}_i is moved, only the curve segment $\mathcal{P}_{i,k}$, which interpolates \mathbf{p}_i and its adjacent curves $\mathcal{P}_{i-1,k}$ and $\mathcal{P}_{i+1,k}$, needs to be updated. This can be achieved by solving the simplified optimization problem defined in Eq. (7), where the involved segments with indices $\eta \in \{i-2, i-1, i\}$ are replaced by $\eta \in \{i-1, i, i+1\}$; see Fig. 8(b). Furthermore, the control points of the segment $\mathcal{P}_{i+1,k}$ that are associated with the continuity constraints $C_{i+1,k}^C$ remains unchanged throughout the optimization process. Similarly, for the specific cases of moving the interpolation points \mathbf{p}_0 or \mathbf{p}_1 (resp., \mathbf{p}_n or \mathbf{p}_{n+1}) for an open $p\kappa$ -curve, only the curves $\mathcal{P}_{1,k}$ and $\mathcal{P}_{2,k}$ (respectively, $\mathcal{P}_{n-1,k}$ and $\mathcal{P}_{n,k}$) are reconstructed (see Fig. 8(a)).

5.2. Initialization method

In the construction of the $p\kappa$ -curve, selecting appropriate initial values for the parameter values \hat{t}_i of the interpolated points \mathbf{p}_i , the parabolas \mathcal{Q}_i , and the curves $\mathcal{P}_{i,k}$ is crucial for the optimizing efficiency and ensuring well-behaved interpolatory curves. In the following, we provide a detailed description of the initialization process for solving the simplified problems in Eqs. (7) and (8). We assume that \mathbf{p}_i has been inserted and continue with the insertion of \mathbf{p}_{i+1} . We label the curve segments obtained after inserting \mathbf{p}_i and before inserting \mathbf{p}_{i+1} as $\hat{\mathcal{P}}_{j,k}$ ($1 \leq j < i$), where \hat{t}_j corresponds to the parameter of interpolation point \mathbf{p}_j .

5.2.1. Open curve initialization

We will begin with the general case $i > 2$ and then address the other special case. As detailed in Section 5.1 and Fig. 6, when inserting \mathbf{p}_{i+1} , the initialization of three curve segments, namely $\mathcal{P}_{i-2,k}$, $\mathcal{P}_{i-1,k}$, and $\mathcal{P}_{i,k}$, is required. This involves determining the control points for these three curves and specifying the initialization parameters \hat{t}_{i-2} , \hat{t}_{i-1} , and \hat{t}_i that correspond to the interpolation points \mathbf{p}_{i-2} , \mathbf{p}_{i-1} , and \mathbf{p}_i , respectively. Below, we discuss the initialization process for constructing G^2/C^2 -continuity curves, noting that the initialization for G^1/C^1 -continuity follows a similar approach.

- **G^2 -continuity.** $\hat{\mathcal{P}}_{i-2,k}$ and \hat{t}_{i-2} directly initialize the curve $\mathcal{P}_{i-2,k}$ and parameter for \mathbf{p}_{i-2} when inserting \mathbf{p}_{i+1} , i.e., $\mathcal{P}_{i-2,k} = \hat{\mathcal{P}}_{i-2,k}$ and $\hat{t}_{i-2} = \hat{t}_{i-2}$. Notably, $\hat{\mathcal{P}}_{i-1,k}$ interpolates both \mathbf{p}_{i-1} and \mathbf{p}_i . However, when inserting \mathbf{p}_{i+1} , $\mathcal{P}_{i-1,k}$ should be initialized to interpolate only \mathbf{p}_{i-1} . To achieve this, we subdivide $\hat{\mathcal{P}}_{i-1,k}$ at the parameter value $z_{i-1} = \frac{1+\hat{t}_{i-1}}{2}$. As shown in Fig. 6(b), the curve $\hat{\mathcal{P}}_{i-1,k}$ in Fig. 6(a) is

split into two curve segments, marked by a solid curve and a dashed curve, respectively. The segment $\hat{\mathcal{P}}_{i-1,k}^{[0,z_{i-1}]}$ is used as the initialization for $\mathcal{P}_{i-1,k}$, and $\hat{t}_{i-1} = \frac{\hat{t}_{i-1}}{z_{i-1}}$. For initializing the parameter of \mathcal{P}_i , we employ the chord length parameterization method, i.e., $\hat{t}_i = \frac{|c_{i-1,k}p_i|}{|c_{i-1,k}p_i|+|p_i p_{i+1}|}$ (as shown in Fig. 6(c)). The last segment is then uniquely initialized to achieve C^2 -continuity with the curve segment $\mathcal{P}_{i-1,k}$ at the joint $c_{i-1,k}$, while also interpolating p_i at $t = \hat{t}_i$ and p_{i+1} at $t = 1$, and satisfying $c_{i,k-1} = \frac{c_{i,k-2} + c_{i,k}}{2}$. Fig. 6(c) provides a visual representation of this process for the three curve segments $\mathcal{P}_{i-2,k}$, $\mathcal{P}_{i-1,k}$, and $\mathcal{P}_{i,k}$ when inserting p_{i+1} , all marked in cyan.

- **C^2 -continuity.** Note that, the G^2 -continuous initialization already achieves G^2 -continuity at $c_{i-2,k} = c_{i-1,0}$, C^2 -continuity at $c_{i-1,k} = c_{i,0}$, and satisfies interpolation constraints. With minor adjustments, it can serve as the initialization for C^2 -continuous curve construction. Specifically, we update $c_{i-2,k} = c_{i-1,0}$ and $c_{i-1,2}$ according to the C^2 -continuity constraints at $c_{i-2,k} = c_{i-1,0}$ while keeping the remaining control points fixed to obtain the C^2 -continuous initialization.

When only three points p_0 , p_1 , and p_2 are inserted, we initialize a single segment $\mathcal{P}_{1,k}$ for interpolation. Specifically, we set $\hat{t}_1 = \frac{\|p_0 p_1\|}{\|p_0 p_1\| + \|p_1 p_2\|}$ and construct a quadratic Bézier curve, $\mathcal{P}_{1,2}$, to interpolate p_0 , p_1 , and p_2 at parameters 0, \hat{t}_1 , and 1, respectively. The curve $\mathcal{P}_{1,2}$ is then elevated to degree- k and serves as the initialization for $\mathcal{P}_{1,k}$. When adding a new point p_3 , a similar method is applied to initialize $\mathcal{P}_{1,k}$ and $\mathcal{P}_{2,k}$ as the one used for initializing $\mathcal{P}_{i-1,k}$ and $\mathcal{P}_{i,k}$ when inserting p_{i+1} .

5.2.2. Closed curve initialization

We now address the initialization of $\mathcal{P}_{n+1,k}$, $\mathcal{P}_{0,k}$, $\mathcal{P}_{1,k}$ in Fig. 7 along with the parameter values \hat{t}_{n+1} , \hat{t}_0 , and \hat{t}_1 . Note that by employing the open curve construction method and treating p_0 as a point inserted subsequent to p_{n+1} , we can achieve a closed curve comprised of $n+1$ Bézier curves $\{\mathcal{P}_{i,k}\}_{i=1}^{n+1}$ that interpolate p_i at \hat{t}_i , respectively. The segments $\hat{\mathcal{P}}_{n+1,k}$ and $\hat{\mathcal{P}}_{1,k}$ are connected with C^0 continuity at p_0 . We subdivide $\hat{\mathcal{P}}_{n+1,k}$ and $\hat{\mathcal{P}}_{1,k}$ at parameters $z_{n+1} = \frac{\hat{t}_{n+1} + 1}{2}$ and $z_1 = \frac{\hat{t}_1}{2}$, respectively. We use the chord length parameterization method and subdivision method to determine the parameters for interpolated points as follows: $\hat{t}_{n+1} = \frac{\hat{t}_{n+1}}{z_{n+1}}$, $\hat{t}_0 = \frac{|c_{0,0}p_0|}{|c_{0,0}p_0| + |p_0 c_{0,k}|}$, and $\hat{t}_1 = \frac{\hat{t}_1}{2-2z_1}$. The initialization for $\mathcal{P}_{n+1,k}$, $\mathcal{P}_{0,k}$, $\mathcal{P}_{1,k}$ that maintain parametric continuity is as follows:

- **C^2 -continuity:** The endpoints of the curve $\mathcal{P}_{0,k}$ are initially set as $c_{0,0} = \hat{\mathcal{P}}_{n+1,k}(z_{n+1})$ and $c_{0,k} = \hat{\mathcal{P}}_{1,k}(z_1)$. Note that there are a total of 18 DOFs for the three curve segments $\mathcal{P}_{n+1,k}$, $\mathcal{P}_{0,k}$ and $\mathcal{P}_{1,k}$, where 3 DOFs are allocated to interpolate p_{n+1} , p_0 , and p_1 at \hat{t}_{n+1} , \hat{t}_0 , and \hat{t}_1 respectively. Three DOFs are allocated to each endpoint $c_{n,k}$ and $c_{1,k}$, ensuring C^2 -continuity at both joints. Meanwhile, an additional 4 DOFs are devoted to each endpoint $c_{0,0}$ and $c_{0,k}$ to attain C^2 -continuity. To finalize the initial curves, we require the curve $\mathcal{P}_{0,k}$ to pass through the point $\frac{c_{0,0} + 2p_0 + c_{0,k}}{4}$ at parameter $t = 0.5$, using the last remaining DOF. An example of the initialization curves $\mathcal{P}_{n+1,k}$, $\mathcal{P}_{0,k}$, and $\mathcal{P}_{1,k}$ satisfying all constraints is shown in Fig. 7(c).
- **C^1 -continuity:** The control point $\bar{c}_{n+1,1}$ (resp. $\bar{c}_{1,k-1}$) of segment $\hat{\mathcal{P}}_{n+1,k}^{[0,z_{n+1}]}$ (resp. $\hat{\mathcal{P}}_{1,k}^{[z_1,1]}$) is adjusted to ensure C^1 continuity with $\mathcal{P}_{0,k}$ at the joint $c_{0,0}$ (resp. $c_{0,k}$). This updated segment then serves as the initialization for $\mathcal{P}_{n+1,k}$ (resp. $\mathcal{P}_{1,k}$). The initialization of $\mathcal{P}_{0,k}$ is uniquely determined by the C^1 -continuity constraints at the endpoints $c_{0,0}$ and $c_{0,k}$, along with the interpolation constraint $\mathcal{P}_{0,k}(\hat{t}_0) = p_0$.

The initialization for constructing closed $p\kappa$ -curves with G^1 - and G^2 -continuity is the same as that for C^1 - and C^2 -continuity, respectively.

5.2.3. Parabola initialization

For each curve $\mathcal{P}_{j,k}$ with $j = i-2, i-1, i$, we obtain the initial values of the coefficients of the corresponding parabola $\{a_{j,2}, a_{j,1}, a_{j,0}\}$ by constrained linear least square fitting technique. Specifically, for each

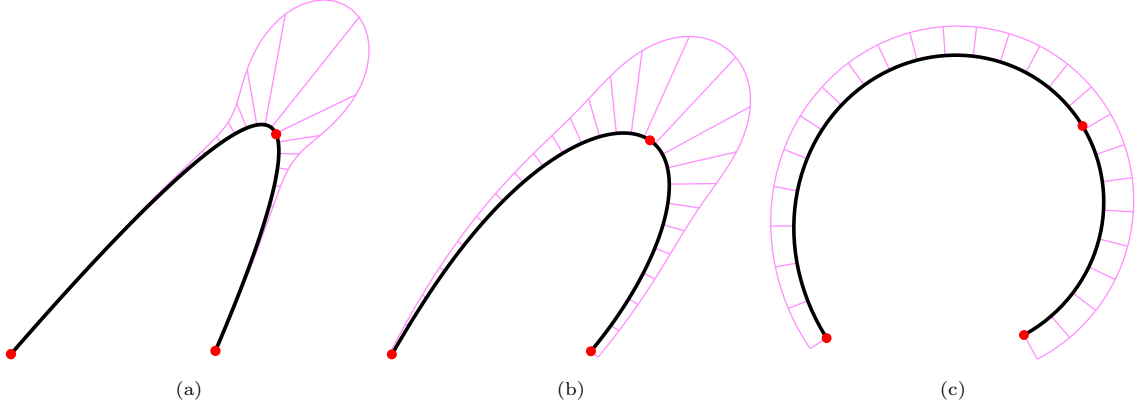


Figure 9: A $p\kappa$ -curve construction process based on the two-stage optimization. (a) Initial curve, and (b&c) results after the first and second stages of optimization. The curve quality is visualized using the curvature comb (pink), and the red points represent the interpolated points.

initial curve $\mathcal{P}_{j,k}$, the associated parabola must possess the axis of symmetry $t = \hat{t}_j = -\frac{a_{j,1}}{2a_{j,2}}$. We compute curvatures for each Bézier curve at s evenly spaced points in the parameter domain. Using the constrained linear least square method, we determine the best-fitting parabola from these curvature samples, which then serves as the initialization for the parabolas. Throughout all our experiments, we set $s = 100$.

5.3. Two-stage optimization approach

The first stage involves formulating the objective functional using the following equation:

$$E_i = E_{i,p} + \lambda_{i,e}E_{i,e} + \lambda_{i,c}E_{i,c}, \quad (9)$$

where $\lambda_{i,e}$ and $\lambda_{i,c}$ are the parameters used to penalize the energy terms $E_{i,e}$ and $E_{i,c}$, respectively. The role of the energy terms $E_{i,e}, E_{i,c}$ is further analysed in Section 6.1, and the parameters $\lambda_{i,e}, \lambda_{i,c}$ are set accordingly. The first stage of optimization aims to mitigate shape changes in curvature and generates a favorable initial value for the second stage of optimization; see Fig. 9(b). In the second stage of our process, we utilize the outcome from the first stage as the initial value for the objective functional (3), which results in the curvature function of the curve becoming closer to a parabola; see Fig. 9(c). Both stages of optimization are terminated if the maximum value of the corresponding energy is less than the prescribed tolerance ϵ or if the number of iterations exceeds the specified number of steps N_{iter} . By following this process, we can ultimately achieve a satisfactory result.

6. Experimental results and comparisons

In this section, we begin by conducting ablation experiments to emphasize the significance of the energy term in Eq. (9). Next, we showcase examples that are constructed using our $p\kappa$ -curves. Finally, we compare our $p\kappa$ -curves with state-of-the-art methods for interactive curve design. All the algorithms presented in this paper were implemented and executed using MATLAB R2023a.

6.1. Ablation study

Besides the parabola curvature term, our optimization energy defined in Eq. (6) also includes an edge length regularization $E_{i,e}$ and a curve length term $E_{i,c}$. These terms penalize the difference between the lengths of adjacent edges of control points and the total curve length, respectively. In this section, we demonstrate the effect of these two energy terms and discuss the selection of corresponding weights $\lambda_{i,e}$ and $\lambda_{i,c}$. All our optimization problems are solved using the interior point algorithm (Byrd et al., 1999). The integrals in the energy are computed by dividing the domain of integration $[0, 1]$ into 100 sub-intervals and

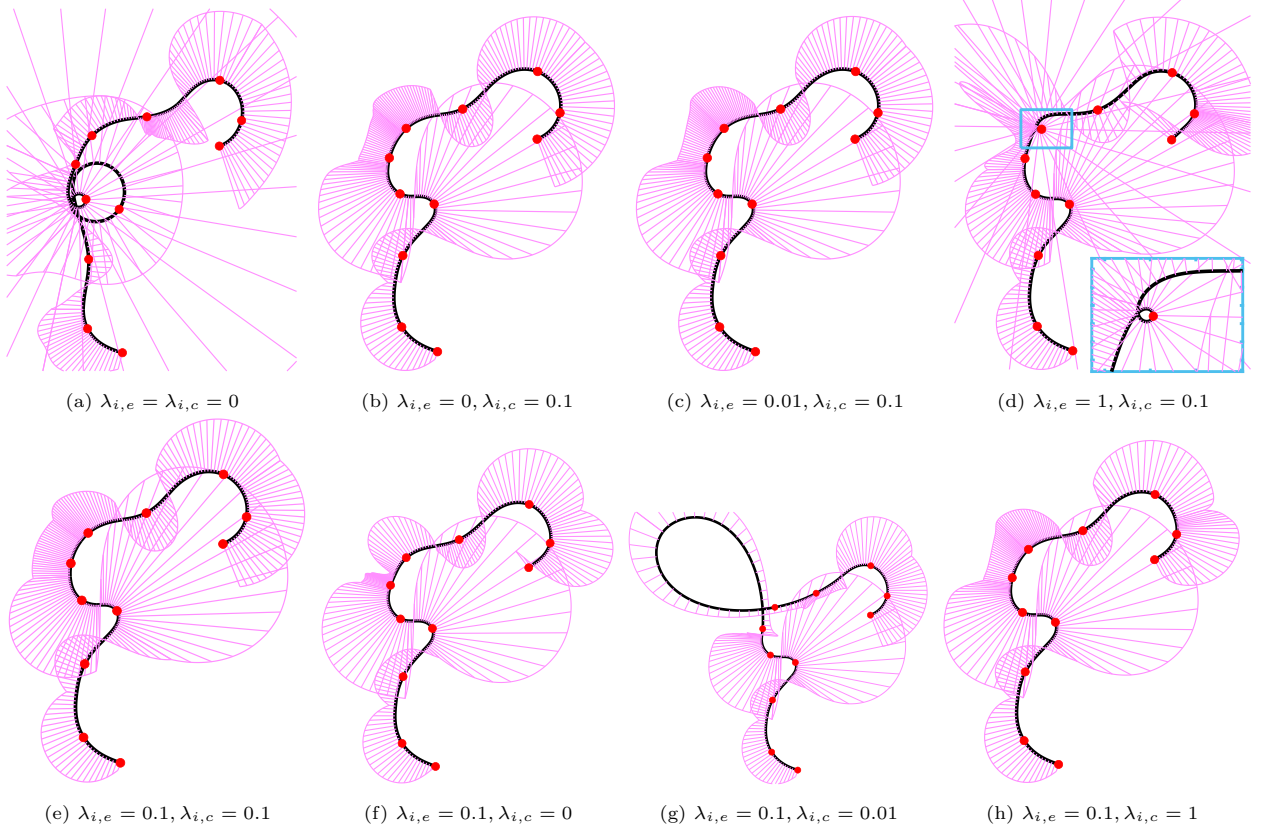


Figure 10: $p\kappa$ -curves for different weights $\lambda_{i,e}$ and $\lambda_{i,c}$, where red points represent the interpolated points. The curve quality is visualized using the curvature comb (pink).

Table 1: Statistics of energies for different weights $(\lambda_{i,e}, \lambda_{i,c})$ in Fig. 10.

	Fig. 10(a)	Fig. 10(b)	Fig. 10(c)	Fig. 10(d)	Fig. 10(e)	Fig. 10(f)	Fig. 10(g)	Fig. 10(h)
$(\lambda_{i,e}, \lambda_{i,c})$	(0, 0)	(0, 0.1)	(0.01, 0.1)	(1, 0.1)	(0.1, 0.1)	(0.1, 0)	(0.1, 0.01)	(0.1, 1)
\bar{E}	8.33×10^{-3}	3.18×10^{-4}	3.02×10^{-4}	1.67×10^{-2}	1.18×10^{-4}	6.51×10^{-4}	2.27×10^{-3}	3.32×10^{-4}
\hat{E}	4.98×10^{-2}	1.56×10^{-3}	1.56×10^{-3}	8.36×10^{-2}	3.24×10^{-4}	4.07×10^{-3}	1.29×10^{-2}	1.52×10^{-3}

Note: The best results in the table are shown in bold font.

applying the composite Simpson's rule (Burden et al., 2015) to each of these sub-intervals. To quantitatively evaluate the approximation of the curvature distribution to a parabola, we introduce two energy measures: the average energy \bar{E} and the maximum energy \hat{E} for each example. These measures are defined as follows:

$$\bar{E} = \frac{1}{N} \sum_{i=1}^N E_{i,p}, \quad \text{and} \quad \hat{E} = \max\{E_{i,p} | i = 1, \dots, N\}, \quad (10)$$

where N is the number of Bézier segments of the interpolatory curve.

First, let us consider the effects of the edge length regularization term and curve length term. In the absence of these terms ($\lambda_{i,e} = \lambda_{i,c} = 0$), the second optimization stage proceeds directly from the initial values. As shown in Fig. 10(a), the resulting curves can become excessively long and self-intersecting. This behavior occurs because, without penalties on edge lengths and overall curve length, the algorithm tends to elongate the curve to reduce curvature, leading to significant length increases. To find appropriate weights

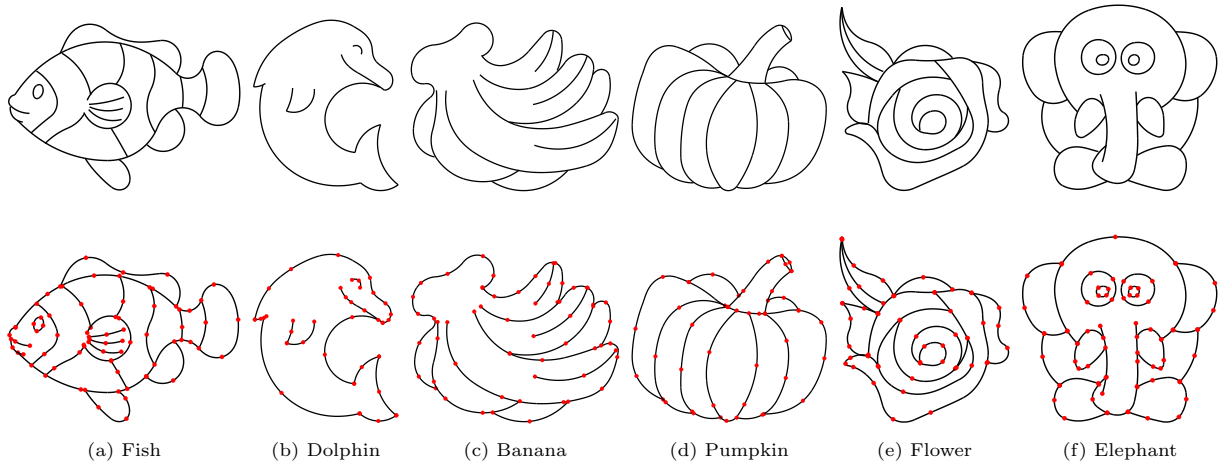


Figure 11: Cartoon graph constructed from $p\kappa$ -curves, where red points represent the interpolation points.

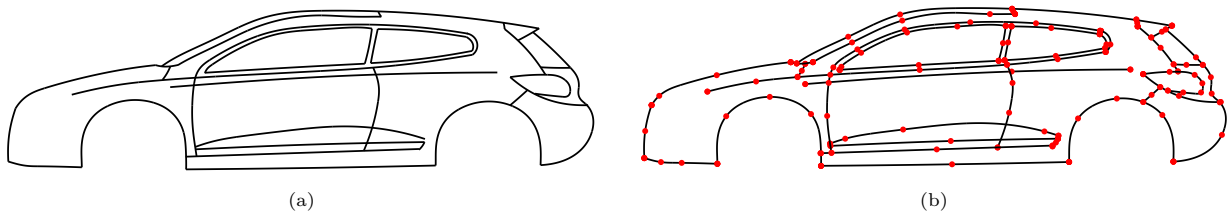


Figure 12: A car model is designed using $p\kappa$ -curves, where red points represent the interpolation points.

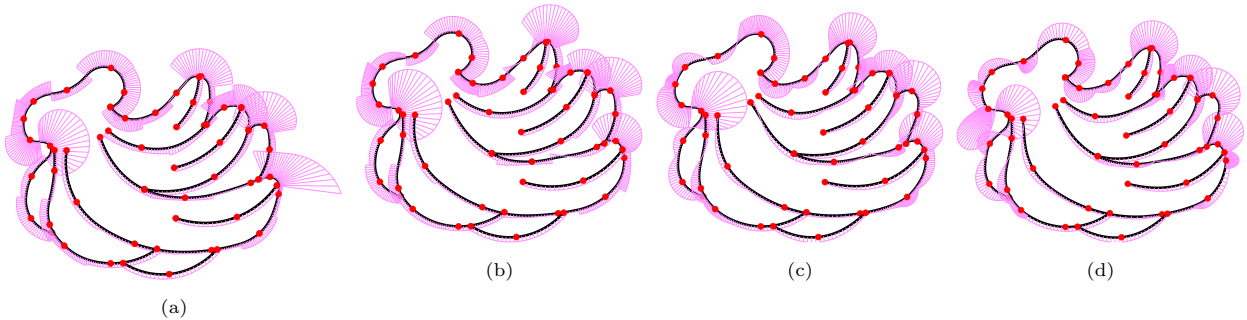


Figure 13: $p\kappa$ -curves with different continuity, where red points represent the interpolation points. (a) C^1 -continuity ($\bar{E} = 6.17 \times 10^{-6}$, $\hat{E} = 1.78 \times 10^{-4}$); (b) G^1 -continuity ($\bar{E} = 1.64 \times 10^{-6}$, $\hat{E} = 4.50 \times 10^{-5}$); (c) C^2 -continuity ($\bar{E} = 6.24 \times 10^{-5}$, $\hat{E} = 1.12 \times 10^{-3}$); (d) G^2 -continuity ($\bar{E} = 3.23 \times 10^{-5}$, $\hat{E} = 7.75 \times 10^{-4}$).

$\lambda_{i,e}$ and $\lambda_{i,c}$ for balanced energy, we first maintain $\lambda_{i,c}$ constant and vary $\lambda_{i,e}$. In Fig. 10(b-e), we show $p\kappa$ -curves for $\lambda_{i,e} = 0, 0.01, 1, 0.1$, while fixing $\lambda_{i,c} = 0.1$. Results suggest that $\lambda_{i,e} \in [0, 0.1]$ works well. However, larger $\lambda_{i,e}$ diminish the impact of curve length, potentially resulting in local self-intersections; see the region enclosed by the blue box in Fig. 10(d). Next, we consider the impact of varying $\lambda_{i,c}$ values on our resultant curves while keeping $\lambda_{i,e}$ fixed at 0.1. The corresponding outcomes are illustrated in Fig. 10(e-h). We note that favorable outcomes are obtained when $\lambda_{i,e}$ falls within the range of $[0, 0.1]$, and $\lambda_{i,c}$ lies within the range of $[0.1, 1]$, as shown in Fig. 10(e&h). In Table 1, we provide statistics for the corresponding average energy \bar{E} and maximum energy \hat{E} with different weight configurations. Given the lower energy value obtained in Fig. 10(e), we consistently set $\lambda_{i,e} = \lambda_{i,c} = 0.1$ across all our examples. This choice well balances the energy terms and yields desirable curve shapes.

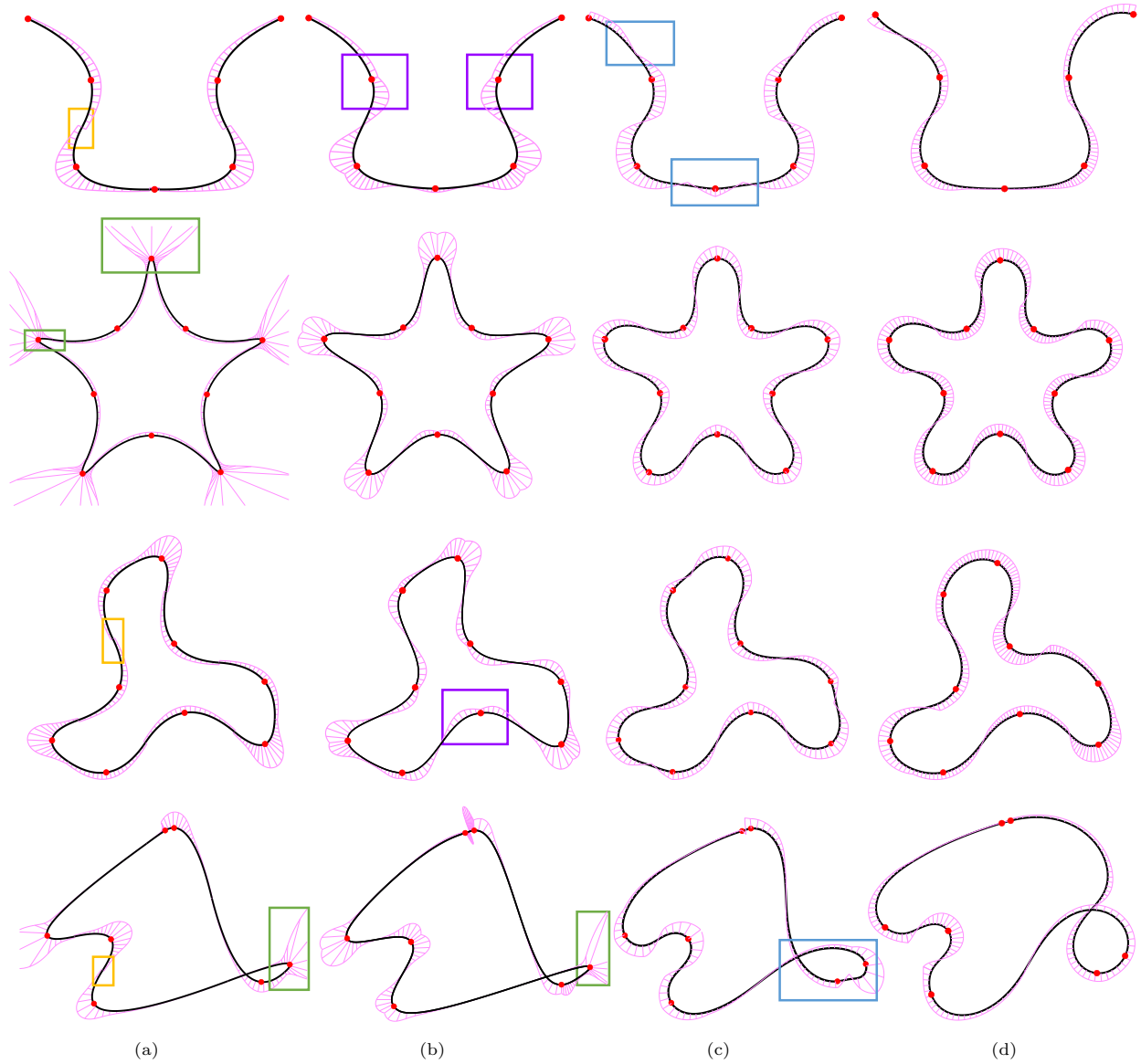


Figure 14: Comparison of $p\kappa$ -curves with other types of interpolation curves, where red points represent the interpolation points. (a) κ -curves (Yan et al., 2017); (b) trigonometric blending curves (Yuksel, 2020); (c) 3-arcs clothoids (Binninger and Sorkine-Hornung, 2022); (d) C^2 -continuous $p\kappa$ -curves. Yellow and green boxes indicate curvature discontinuities and abrupt changes, respectively. Purple boxes enclose interpolation points that are not located at curvature extremes, while blue boxes enclose segments with curvatures exhibiting multiple monotonic intervals.

6.2. Results

In this section, we demonstrate the application of $p\kappa$ -curves in cartoon drawing and CAD sketching. Fig. 11 illustrates a cartoon graph constructed using multiple quartic $p\kappa$ -curves with C^1 -continuity. The interpolation points used for constructing the curves are presented in the second row. Fig. 11(d-f) are specifically designed with reference to the literature (Yan et al., 2017). Fig. 12 showcases a car profile drawing created using quintic C^2 $p\kappa$ -curves. The design of the car profile is based on the work (Havemann et al., 2013). It is evident that $p\kappa$ -curves consistently produce a visually fair and aesthetically pleasing result. Our method allows for the generation of $p\kappa$ -curves with different geometric and parametric continuity orders. This can be achieved by specifying the desired curve order and corresponding constraints in the optimization problem. Fig. 13 depicts curves with different continuity orders generated for the same interpolated point sequence. The curvature comb is used to better visualize the differences between the results. The statistics of all the examples shown in Figs. 11, 12 and 14 are summarized in Table 2. The average energy \bar{E} for all the curves is less than 2.00×10^{-3} . The average computation time for inserting a single point is less than 0.83 seconds. Furthermore, curves with geometric continuity generally have more DOFs compared to curves with the same order of parametric continuity. This increased flexibility often enables the achievement of lower energy values in the optimization process.

6.3. Comparisons

In this section, we compare our curves with three state-of-the-art interpolation curves, namely κ -curves (Yan et al., 2017), trigonometric blending curves (Yuksel, 2020), and 3-arcs clothoid (Binninger and Sorkine-Hornung, 2022), in terms of continuity, locality, and fairness.

Continuity. As demonstrated earlier, our method enables the generation of C^1 -, C^2 -, G^1 -, and G^2 -continuous $p\kappa$ -curves. The κ -curve, which is also composed of Bézier curves, achieves only G^1 -continuity. This is illustrated in Fig. 14(a), where the curvature of the κ -curve exhibits discontinuities at the inflection points; see the area enclosed by the yellow box. While trigonometric blending curves and 3-arcs clothoids can achieve C^2 -continuity, it is important to note their limitations. Trigonometric blending curves use non-polynomial blend functions involving trigonometric functions, which can be computationally expensive and impractical for traditional CAD systems. Similarly, the representation of 3-arcs clothoids relies on Fresnel integrals, which are transcendental functions and may not be easily integrated into CAD systems. In contrast, our $p\kappa$ -curves provide a polynomial-based representation, making them more suitable for practical CAD applications.

Fairness. The κ -curves and trigonometric blending curves are constructed by splicing and blending quadratic Bézier curves, respectively. Quadratic Bézier curves have limited degrees of freedom, which can make it challenging to control the variation of curvature along the curve, leading to abrupt changes in curvature and undesired visual appearance, as highlighted in the green boxes in Fig. 14(a). $p\kappa$ -curves exhibit more uniform curvature variation, avoiding abrupt changes in curvature and resulting in visually smoother curves. Moreover, for trigonometric blending curves, we observe that the interpolated points are generally not located at the curvature extremes, as highlighted by the purple boxes in Fig. 14(b). For 3-arcs clothoids, there are multiple curve segments (highlighted by the blue boxes) with curvatures that contain multiple monotonic intervals; see Fig. 14(c). The use of 3-arcs clothoids guarantees the monotonicity of curvature between interpolation points with opposite curvature signs. However, when there are interpolation points with the same curvature sign, it leads to more variation in the curvature and can result in an unsatisfactory shape for the curve. The curvature distribution of our $p\kappa$ -curves tends to have at most two distinct monotonic intervals, which results in a more aesthetically pleasing curve shape; see Fig. 14(d).

Locality. In Fig. 15, we compare the influence of moving one interpolating point when using different curves to interpolate the same sequence of points. Since κ -curves rely on global optimization methods, there is no guarantee that they possess locality (Yan et al., 2017). In our experiments, we find that the influence of moving an interpolation point on the κ -curve is obvious on the segments between at least six neighboring interpolated points around the interpolation point; see Fig. 15(a). In the case of trigonometric blending curves (Yuksel, 2020), each curve is obtained by blending two arcs that interpolate between three consecutive points. As a result, when an interpolation point changes position, it affects the shape of the portion between

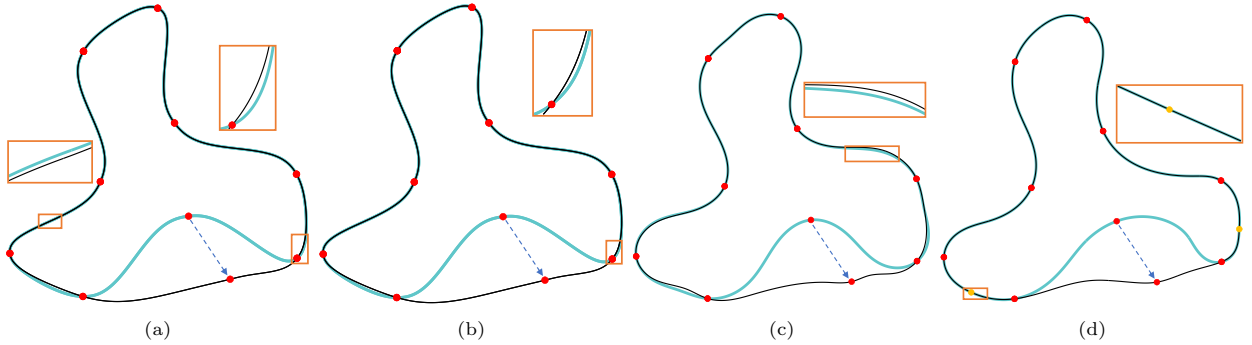


Figure 15: Comparison of locality when moving one interpolation point, where red points represent the interpolation points. The updated segments are colored in cyan. (a) κ -curves (Yan et al., 2017); (b) trigonometric blending curves (Yuksel, 2020); (c) 3-arcs clothoids (Binninger and Sorkine-Hornung, 2022); (d) $p\kappa$ -curve.

Table 2: Statistics of $p\kappa$ -curve for examples in Fig. 11, Fig. 12 and Fig. 14

Example	N_I	N_O	N_C	\bar{E}	\hat{E}	$T(sec.)$
Fig. 11(a)	78	18	1	8.36×10^{-5}	1.75×10^{-3}	0.11
Fig. 11(b)	43	11	0	1.78×10^{-6}	1.74×10^{-5}	0.15
Fig. 11(c)	59	10	0	3.60×10^{-4}	7.08×10^{-3}	0.22
Fig. 11(d)	52	10	0	1.28×10^{-6}	2.13×10^{-5}	0.16
Fig. 11(e)	59	11	0	1.64×10^{-6}	4.50×10^{-5}	0.18
Fig. 11(f)	76	11	4	4.26×10^{-6}	1.14×10^{-4}	0.23
Fig. 12	141	35	0	4.45×10^{-5}	9.42×10^{-4}	0.76
Fig. 14(first row)	7	1	0	4.16×10^{-4}	9.63×10^{-4}	0.26
Fig. 14(second row)	10	0	1	1.73×10^{-3}	2.94×10^{-3}	0.28
Fig. 14(third row)	9	0	1	9.96×10^{-4}	3.14×10^{-3}	0.28
Fig. 14(fourth row)	7	0	1	1.81×10^{-3}	4.99×10^{-3}	0.83

Note: N_I denotes the number of interpolated points, N_O denotes the number of open curves, N_C denotes the number of closed curves, and T denotes the average time to insert a point.

the five neighboring interpolated points; see Fig. 15(b). On the other hand, for 3-arcs clothoids, when the position of an interpolation point changes, the portion between the 6 or 8 neighboring interpolated points is affected, depending on the chosen curvature estimation method (Binninger and Sorkine-Hornung, 2022); see Fig. 15(c). In contrast, when changing the position of an interpolation point, our curves only undergo a shape change in at most three Bézier segments that interpolate the two nearest neighbor interpolated points; see the segment between two joints marked with yellow points in Fig. 15(d).

7. Conclusion

This paper introduces a novel class of smooth interpolation curves called $p\kappa$ -curves. The $p\kappa$ -curves are constructed by joining multiple segments of Bézier curves, with each segment exhibiting a curvature distribution that approximates a parabola. $p\kappa$ -curves can achieve the desired continuity orders such as C^1 , C^2 , G^1 , and G^2 and demonstrate improved localizability. They also exhibit a more aesthetically pleasing appearance and a more uniformly distributed curvature compared to existing G^2 -continuous curves. The interpolated points of a $p\kappa$ -curve approximately correspond to the extrema of the segment's curvature, which provides designers with an intuitive mean to manipulate the shape of the curve. Several experiments have showcased the successful application of $p\kappa$ -curves in designing a wide range of shapes, demonstrating their

potential in both artistic and industrial design domains.

One limitation of our $p\kappa$ -curves is that we cannot ensure symmetric shapes even when the input data is symmetric. This is due to the localized nature of our optimization method. While global optimization might improve results, it often comes at the expense of increased computational costs. Therefore, it is valuable to explore more advanced optimization methods that achieve a better balance between shape symmetry and computation time. On the other hand, as we use Bézier curves as primitives in our method, our curves are unable to accurately represent conics, which are commonly used in industries. Therefore, it is worth exploring the extension of our $p\kappa$ -curves to include other geometric primitives, such as rational Bézier curves, to enhance the shape representation ability. Additionally, considering the 3D cases and accounting for torsion variations would further enhance the capabilities and applicability of $p\kappa$ -curves.

Acknowledgments

The research of Juan Cao was supported by the National Natural Science Foundation of China (No. 62272402) and the Fundamental Research Funds for the Central Universities (No. 20720220037). The research of Zhong-gui Chen was supported by the National Natural Science Foundation of China (Nos. 61972327 and 62372389) and Natural Science Foundation of Fujian Province (No. 2022J01001).

References

- Atneave, F., 1954. Some informational aspects of visual perception. *Psychological Review* 61, 183.
- Barry, P.J., Goldman, R.N., 1988. A recursive evaluation algorithm for a class of Catmull-Rom splines. *Siggraph Computer Graphics* 22, 199–204.
- Bertolazzi, E., Frego, M., 2018. Interpolating clothoid splines with curvature continuity. *Mathematical Methods in the Applied Sciences* 41, 1723–1737.
- Binninger, A., Sorkine-Hornung, O., 2022. Smooth interpolating curves with local control and monotone alternating curvature. *Computer Graphics Forum* 41, 25–38.
- Burden, R.L., Faires, J.D., Burden, A.M., 2015. *Numerical Analysis*. Cengage Learning.
- Byrd, R.H., Hribar, M.E., Nocedal, J., 1999. An interior point algorithm for large-scale nonlinear programming. *SIAM Journal on Optimization* 9, 877–900.
- Cao, J., Wang, G., 2008. A note on Class A Bézier curves. *Computer Aided Geometric Design* 25, 523–528.
- Catmull, E., Rom, R., 1974. A class of local interpolating splines, in: Barnhill, R.E., Riesenfeld, R.F. (Eds.), *Computer Aided Geometric Design*. Academic Press, New York, pp. 317–326.
- Chan, C.L., Abbas, M., Ali, J.M., 2011. Minimum energy curve in polynomial interpolation. *MATEMATIKA: Malaysian Journal of Industrial and Applied Mathematics*, 159–167.
- Chen, Z., Huang, J., Cao, J., Zhang, Y.J., 2019. Interpolatory curve modeling with feature points control. *Computer-Aided Design* 114, 155–163.
- Deslauriers, G., Dubuc, S., 1989. Symmetric iterative interpolation processes, in: DeVore, R.A. (Ed.), *Constructive Approximation: Special Issue: Fractal Approximation*. Springer, Boston, pp. 49–68.
- ERİŞKİN, H., YÜCESAN, A., 2016. Bézier curve with a minimal jerk energy. *Mathematical Sciences and Applications E-Notes* 4, 139–148.
- Farin, G., 2002. *Curves and surfaces for CAGD: A practical guide*. Morgan Kaufmann, San Francisco.
- Farin, G., 2006. Class a Bézier curves. *Computer Aided Geometric Design* 23, 573–581.
- Gferrer, A., Röschel, O., 2001. Blended Hermite interpolants. *Computer Aided Geometric Design* 18, 865–873.
- Havemann, S., Edelsbrunner, J., Wagner, P., Fellner, D., 2013. Curvature-controlled curve editing using piecewise clothoid curves. *Computers & Graphics* 37, 764–773.
- Hoschek, J., Lasser, D., Schumaker, L.L., 1993. *Fundamentals of Computer Aided Geometric Design*. A. K. Peters, Ltd, Natick.
- Jiang, Y., Lin, H., Huang, W., 2023. Fairing-PIA: Progressive-iterative approximation for fairing curve and surface generation. *The Visual Computer*, 1–18.
- Johnson, H.S., Johnson, M.J., 2020. Quasi-elastic cubic splines in \mathbb{R}^d . *Computer Aided Geometric Design* 81, 101893.
- Levien, R., Séquin, C.H., 2009. Interpolating splines: Which is the fairest of them all? *Computer-Aided Design and Applications* 6, 91–102.
- Levien, R.L., 2009. *From Spiral to Spline: Optimal Techniques in Interactive Curve Design*. Ph.D. thesis. EECS Department, University of California, Berkeley. Berkeley.
- Mineur, Y., Lichah, T., Castelain, J.M., Giaume, H., 1998. A shape controlled fitting method for Bézier curves. *Computer Aided Geometric Design* 15, 879–891.
- Miura, K., Gobithaasan, R., 2014. Aesthetic curves and surfaces in computer aided geometric design. *International Journal of Automation Technology* 8, 304–316.
- Miura, K.T., Gobithaasan, R., Salvi, P., Wang, D., Sekine, T., Usuki, S., Inoguchi, J.i., Kajiwara, K., 2022. $\epsilon\kappa$ -curves: Controlled local curvature extrema. *The Visual Computer* 38, 2723–2738.

- Miura, K.T., Shibuya, D., Gobithaasan, R.U., Usuki, S., 2013. Designing Log-aesthetic splines with G^2 continuity. *Computer-Aided Design and Applications* 10, 1021–1032.
- Miura, K.T., Sone, J., Yamashita, A., Kaneko, T., 2005. Derivation of a general formula of aesthetic curves, in: *Proceedings of the Eighth International Conference on Humans and Computers (HC2005)*, pp. 166–171.
- Olver, F.W., 2010. *NIST handbook of mathematical functions* hardback and CD-ROM. Cambridge university press.
- Overhauser, A.W., 1968. Analytic definition of curves and surfaces by parabolic blending. Technical Report No: SL 68-40 .
- Piegl, L., Tiller, W., 1996. *The NURBS Book*. Springer Science & Business Media.
- Pobegailo, A.P., 1992. Geometric modeling of curves using weighted linear and circular segments. *The Visual Computer* 8, 241–245.
- Pobegailo, A.P., 2013. Interpolating rational Bézier spline curves with local shape control. *International Journal of Computer Graphics & Animation* .
- Sederberg, T.W., 2012. *Computer aided geometric design*. Course Notes.
- Séquin, C.H., Lee, K., Yen, J., 2005. Fair, G^2 -and C^2 -continuous circle splines for the interpolation of sparse data points. *Computer-Aided Design* 37, 201–211.
- Sun, C., Zhao, H., 2009. Generating fair, C^2 continuous splines by blending conics. *Computers & Graphics* 33, 173–180.
- Szilvási-Nagy, M., Vendel, T.P., 2000. Generating curves and swept surfaces by blended circles. *Computer Aided Geometric Design* 17, 197–206.
- Tong, W., Chen, M., 2021. A sufficient condition for 3D typical curves. *Computer Aided Geometric Design* 87, 101991.
- Tsuchie, S., 2023. Reconstruction of aesthetically smooth curves. *The Visual Computer* 39, 353–365.
- Wang, D., Gobithaasan, R., Sekine, T., Usuki, S., Miura, K., 2020. Interpolation of point sequences with extremum of curvature by Log-aesthetic curves with G^2 continuity. *Computer-Aided Design and Applications* 18, 399–410.
- Wang, W., Zhang, Y., 2010. Wavelets-based NURBS simplification and fairing. *Computer Methods in Applied Mechanics and Engineering* 199, 290–300.
- Wenz, H.J., 1996. Interpolation of curve data by blended generalized circles. *Computer Aided Geometric Design* 13, 673–680.
- Wiltsche, A., 2005. Blending curves. *Journal for Geometry and Graphics* 9, 67–75.
- Xu, G., Wang, G., Chen, W., 2011. Geometric construction of energy-minimizing Bézier curves. *Science China Information Sciences* 54, 1395–1406.
- Yan, Z., Schiller, S., Schaefer, S., 2019. Circle reproduction with interpolatory curves at local maximal curvature points. *Computer Aided Geometric Design* 72, 98–110.
- Yan, Z., Schiller, S., Wilensky, G., Carr, N., Schaefer, S., 2017. κ -curves: Interpolation at local maximum curvature. *ACM Transactions on Graphics (TOG)* 36, 1–7.
- Yuksel, C., 2020. A class of C^2 interpolating splines. *ACM Transactions on Graphics (TOG)* 39, 1–14.
- Zhang, C., Zhang, P., Cheng, F.F., 2001. Fairing spline curves and surfaces by minimizing energy. *Computer-Aided Design* 33, 913–923.